Journal of Magnetism and Magnetic Materials 564 (2022) 170042

Contents lists available at ScienceDirect

Journal of Magnetism and Magnetic Materials

journal homepage: www.elsevier.com/locate/jmmm

Research article

The meaning of maxima and minima in first order reversal curves: Determining the interaction between species in a sample

R. Moreno [a,*], W. Williams [a], A.R. Muxworthy [b], G.A. Paterson [c], D. Heslop [d]

[a] Earth and Planetary Science, School of Geosciences, University of Edinburgh, Edinburgh, UK
[b] Department of Earth Science and Engineering, Imperial College London, London, UK
[c] Department of Earth, Ocean and Ecological Sciences, University of Liverpool, Liverpool, UK
[d] Research School of Earth Science, The Australian National University, Canberra, Australia

ARTICLE INFO

Keywords:
Nanomagnetism
FORCs
Magnetic-interactions
Nanowires
Single-domain

ABSTRACT

First-order reversal curves (FORCs) are a characterization technique for magnetic materials used in a wide range of research fields. Since their first application in the Earth Sciences two decades ago, their importance in science has been continuously growing and new experimental techniques have been subsequently designed based on the original idea of FORCs. Nonetheless, very recent experimental works on very well designed and simple magnetic structures demonstrate that even for the most simple cases the interpretation of FORC data lacks understanding. In this work, we address this problem analytically, explaining the meaning of maxima, minima and noisy tails and set a strategy to extract the interaction field between magnetic structures. The origin of this interaction field is often the magnetostatic energy, however, we propose that this strategy could be applied for estimating exchange interactions too.

1. Introduction

First-order reversal curves (FORCs) are a characterization method for hysteretic materials originally developed for identifying magnetic domain states of natural samples used in paleomagnetic studies [1,2]. Due to their simplicity and potential application to other disciplines, the use of FORCs rapidly spread to other research fields in which characterization of hysteresis behavior, in particular magnetic hysteresis, plays a central role [3–9]. Nevertheless, after two decades of experimental application, many theoretical investigations [10–13] and even the development of novel techniques extending the original FORC concept (SORCs, tFORCs, rFORCs etc.) [14–17] there still exists a lack of understanding as to how to comprehensively interpret experimental FORC data.

FORCs are an extended version of major Hysteresis Loop analysis. A hysteresis loop measures the path of the magnetization as a function of an external magnetic field; typically the field is varied from a positive field (H_S) sufficient to yield a saturation magnetization (M_S), to a negative saturating field. This yields a 2-dimensional data set $m(H_A)$, where H_A represents the magnetic fields at which the magnetization (M) has been measured and $m = M/M_S$ is the reduced magnetization. Starting from a positively saturated state, FORCs are a series of partial hysteresis curves, where the magnetic field is reversed at H_A, before negative saturation is reached [2]. This yields a 3-dimensional data set $m(H_A, H_B)$, where H_B represents the magnetic field values along each FORC. The FORCs map out the interior of the hysteresis loop, recording more information than the major hysteresis loop alone.

Contrary to a hysteresis loop measurement where $m(H_A)$ is used to represent the magnetic properties of a given material, and often characterized in terms of parameters such as saturation, remanence, coercive force and squareness [18–20], in FORC analysis the unprocessed $m(H_A, H_B)$ measured data are rarely displayed [21–23]. Instead, the second mixed derivative of $m(H_A, H_B)$ is calculated to obtain the FORC function $\rho(H_A, H_B) = -\frac{1}{2}\frac{\partial^2 m(H_A,H_B)}{\partial H_A \partial H_B}$. $\rho(H_A, H_B)$ is displayed as a contour plot [2]. This plot is commonly presented with a 45° rotation with the (H_A, H_B) axes replaced by (H_C, H_U), where the H_C axis corresponds to $-H_A = H_B$, and the H_U to $H_A = H_B$. The simplest case of a FORC diagram $\rho(H_A, H_B)$ for a hysteretic magnetic material is a contour plot in which all values are null, but a single positive peak located on the H_C axis.

Interpreting the meaning of $\rho(H_A, H_B)$ is the main task in FORC analysis. For instance, in paleomagnetism, the shape of this maximum is used to identify the magnetic domain states, e.g., single domain (SD), pseudo-single domain or multidomain (MD), of the magnetic minerals contributing to the magnetic signal of a sample [24,25]. Such information can be used to characterize the recording fidelity of the remanent magnetization in rocks [26,27]. The positions of maxima on

* Corresponding author.
E-mail address: roberto.moreno@ed.ac.uk (R. Moreno).

https://doi.org/10.1016/j.jmmm.2022.170042
Received 8 June 2022; Received in revised form 23 September 2022; Accepted 3 October 2022
Available online 14 October 2022

the H_C axis are assumed to represent the switching field distribution while the distribution in the H_U axis is used to identify and potentially quantify magnetic interactions between magnetic structures [28,29]. However, FORC diagrams are usually more complicated than simple contour plots with a single maximum. FORCs often consist of several prominent maxima and minima (negative peaks), often with noisy 'tails'. The meaning of all features in the FORC distributions are not fully explained in the literature or their explanation is still debated (e.g., the case of minima [30,31]).

Recently, FORCs have been applied to very simple and well defined magnetic structures with the aim of addressing a comprehensive understanding of the different signals a FORC diagram could exhibit. Some examples are two parallel nano-stripes with a tunable distance between them [31], parallel micro-wires [32] or a coreshell microwire [33]. These three examples demonstrate that there are still clear gaps in our understanding of FORC distributions, even though their widespread use over last two decades in range of different systems. For example, these three articles show there exist more maxima than magnetic structures, that the position of those maxima clearly differ from their expected coercive fields, and that the presence of negative peaks lack explanation.

To address this problem, we present a simple analytical study of two interacting nanostructures that can be directly compared with the experimental results in [31–33]. We interpret the different FORC signals that appear in our results, including the minima, and provide a strategy to determine the interaction field between two simple magnetic structures.

2. Model

We consider the analytical study of a simple and well-defined magnetic system: two elongated magnetic nanostructures (NS_1 and NS_2) set parallel to each other and with uniaxial magnetic anisotropy along the elongation axis. The nanostructures are not identical, and we set the magnetization and the coercive field of NS_1 and NS_2 as $M_1 = 2M_2$ and $H_{C2} = 5H_{C1}$. Specifically, coercive fields are taken as $H_{C1} = 10$ and $H_{C2} = 50$ arbitrary units (a.u.). The saturation magnetization (M_S) of both NS is the same, however, it is considered that their cross section area is not. Thus, the wider NS (NS_1) has larger M but lower coercive field. The length of both structures is the same and each NS is assumed to be uniformly magnetized.

The distance separating the nanostructures determines the strength of the interaction field (H_{int}) acting between them due to their respective dipole fields. The strength of the interacting field of NS_1 acting on NS_2 (H_{int1-2}) is different to the reciprocal H_{int2-1}. For simplicity, we consider the mean interaction field $H_{int} = (H_{int1-2} + H_{int2-1})/2$ acts equally on both NS. The existence of H_{int} modifies the intrinsic coercive fields H_C of each NS to the real observed one in a experiment H'_C as $H'_{C1} = H_{C1} \pm H_{int}$ and $H'_{C2} = H_{C2} + H_{int}$ respectively. The interaction field favors the anti-parallel magnetization configuration. Because NS_1 has the lower H_C, it can be either augmented or reduced by the interaction field while NS_2 is always augmented. Specifically, the interaction field reduces the applied magnetic field required to produce the antiparallel magnetic configuration as $|H_{C1}| \rightarrow |H'_{C1}| = |H_{C1}| - |H_{int}|$ and increases the corresponding one to create the parallel configuration as $|H_{C1}| \rightarrow |H'_{C1}| = |H_{C1}| + |H_{int}|$ or $|H_{C2}| \rightarrow |H'_{C2}| = |H_{C2}| + |H_{int}|$. In this work, we consider two extreme cases for the distance between the nanostructures: (1) they are isolated so as to be non-interacting ($H_{int} = 0$ a.u.), and (2) the distance between them is close enough to be strongly interacting (i.e., $H_{int} = 10$ a.u.). These two considerations mimic the experimental configurations presented in [31,32]. Analytical FORC solutions are easily constructed for such a system using the method of Heslop and Muxworthy [34] for regularly gridded data $m(H_A, H_B)$.

The procedure to calculate $m(H_A, H_B)$ for both cases mimics the experimental method. The magnetization of the system is first saturated with a strong magnetic field ($H_S = 80$ a.u in our case). The strength of the field is then decreased in steps of $\Delta H = 1$ a.u. (i.e., the H_A field values). For each H_A value a minor loop is created by increasing the field from H_A to the saturating field, determining the magnetization along this path in steps of $\Delta H = 1$ a.u. (i.e., the H_B values). Each of these 'paths' is an individual FORC, where the magnetization is expressed as $m(H_A, H_B)$; the magnetization values at $H_B = H_A$ match the major branch of the hysteresis loop. In Figs. 1a and 2a we plot $m(H_B)$ versus H_B (i.e., each individual FORC). This is why there are multiple values of magnetization for each H_B field value.

3. Results

Results for the non-interacting case ($H_{int} = 0$ a.u.) are shown in Fig. 1. Fig. 1a displays the $m(H_A, H_B)$ values in a hysteresis-like plot. The upper branch of the major loop is highlighted in red, while the different FORCs are shown in blue diamonds. Green arrows indicate the path of the magnetization. Fig. 1b represents the same information as Fig. 1a but in a heat map that more easily identifies the domain state of the system, with different colors representing the total magnetization and consequently each of the different possible magnetic states. These domain states are also indicated by pairs of arrows representing the magnetization of NS_1 and NS_2. The longer arrow, the bigger M, with the color of the arrows representing NS_1 and NS_2, black and blue, respectively. Fig. 1c represents the corresponding FORC density $\rho(H_A, H_B)$.

The FORC density $\rho(H_A, H_B)$ exhibits two maxima, labeled as H_{C1} and H_{C2}. The positions H_A and H_B of the maxima match the coercive fields of the non-interacting magnetic structures NS_1 and NS_2, hence, their names. The FORC density value at H_{C1} (~ 0.12 a.u) is higher than that at H_{C2} (~ 0.06 a.u) because $M_1 > M_2$. The position of these peaks is highlighted in Fig. 1b with circles labeled as T_1 and T_2 respectively. Comparing both plots, it can be seen that there exists a positive FORC signal (maximum) only at the points where threshold (domain-switching) fields exist in both H_A and H_B.

Starting from a positive saturation field value, the magnetization of both structures points parallel to the (positive) field direction (yellow region). The field needs to be decreased below $-H_{C1}$ (i.e., $H_A \leq -H_{C1}$) to switch the magnetization of NS_1 into the anti-parallel configuration indicated by the orange region. If the field H_A is decreased below $-H_{C2}$, then NS_2 also reverses and the parallel configuration in the negative field direction is achieved (green region). On increasing the magnetic field in the positive direction, NS_1 magnetization switches back at $H_B \geq H_{C1}$, either from the parallel (green region) or anti-parallel configuration (orange region). This remains true even if we decrease H_A beyond that shown in our plot. Therefore, the minimum fields required to produce the magnetization switching away from, and back to the magnetically positive NS_1 state are $H_A = -H_{C1}$ and $H_B = H_{C1}$, respectively, and it is at this position that the maximum H_{C1} appears in Fig. 1c. The same explanation applies the FORC maximum at H_{C2}, which is related to the switching of NS_2. Thus, we can define the maxima in Fig. 1c as the beginning of the transitions T_1 and T_2 in Fig. 1b.

Introducing the interaction field ($H_{int} = 10$ a.u) significantly alters the magnetic behavior of the system (Fig. 2) compared to the non-interacting case (Fig. 1). In this case the FORC diagram (Fig. 2c) exhibits 3 different maxima as well as a minimum. We also show for comparison the non-interaction maxima as black dots that demonstrates that neither of these match the intrinsic coercive fields of the interacting nanostructures. The position of the three maxima are highlighted in Fig. 2b with circles labeled as T_1, T_2 and T_3, and the minimum with a cross also labeled as T_1.

Starting from a positive saturation field value (Fig. 2b), the magnetic domains of the interacting system align parallel to the positive field direction (yellow region). The field needs to be decreased only to $-H'_{C1} = -H_{C1} + H_{int}$, i.e., $H_A \leq -H'_{C1}$, in order to switch the

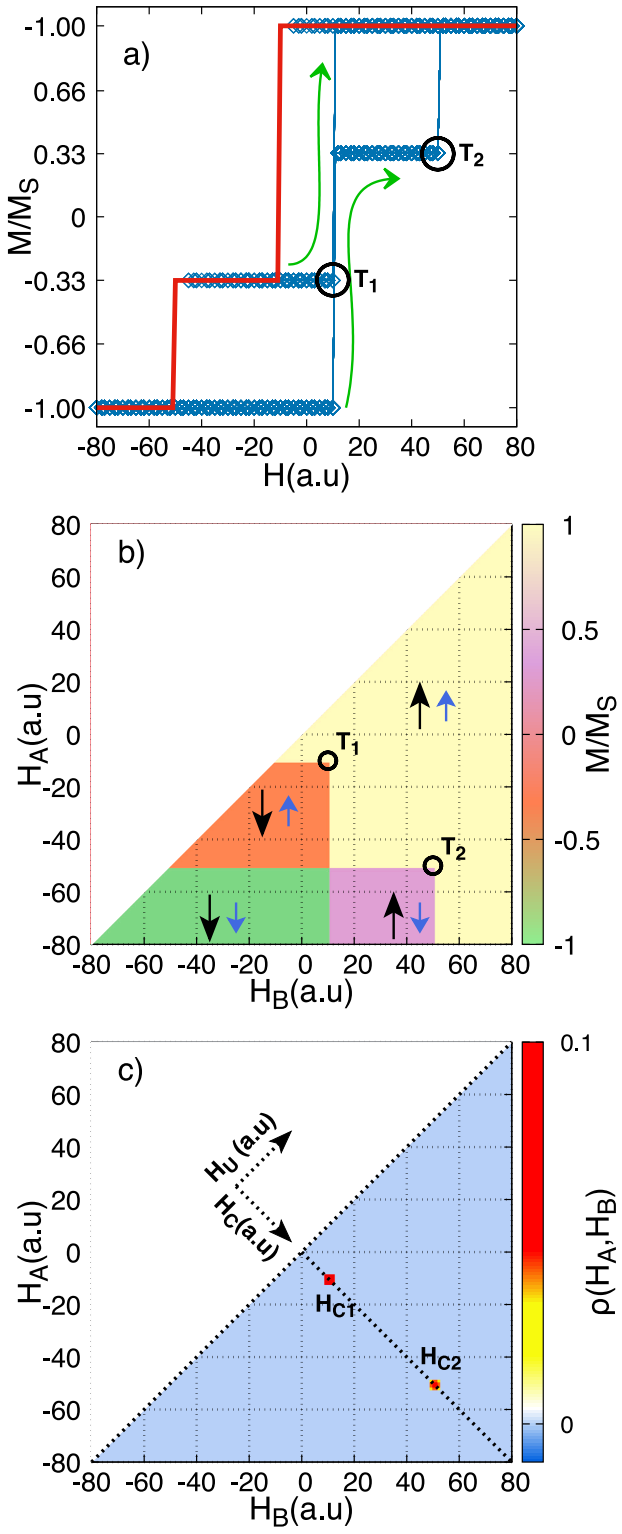

Fig. 1. Non-interacting case. (a) Magnetization versus field in a hysteresis loop like plot. The red line depicts the upper branch of the hysteresis loop, and the blue line and symbols the FORCs. Green arrows indicate the path of the magnetization. (b) Magnetization colormap in terms of the applied field (H_A) and the FORC (H_B). The upper white triangle is outside measurement space. Arrow pairs indicates the magnetic state of the system in the corresponding color region. Black and blue arrow correspond to NS_1 and NS_2 respectively. Black circles highlight the starting H_A and H_B values required to produce a magnetic transition (T_1 or T_2). (c) FORC density plot; interaction H_U and coercive axes H_C are displayed for completeness.

magnetization of NS_1 and create an antiparallel configuration (orange region). In order to switch the magnetization of NS_2 to form the negative parallel configuration (green region), the field needs decrease to $-H'_{C2} = -H_{C2} - H_{int}$. Magnetostatic interactions prevent NS_1 from switching at the same field value H_B independently of the H_A value, as observed in the non-interacting case (Fig. 1). With interactions, switching from the antiparallel configuration (orange region) to the positive parallel state (yellow region) occurs at $H_B \geq H_{C1} + H_{int}$, and switching back from the negative parallel configuration (green region) to the antiparallel state (purple region) occurs at $H_B \geq H_{C1} - H_{int}$. Thus, NS_1 does not always switch to the positive state at the same H_B value, but it will vary with H_A. These two features give rise to the two maxima T_1 and T_2 in the FORC diagram in Fig. 2c. Notice that T_1 starts at the position as the circle labeled as T_1 in Fig. 2b is, and it remains at the same H_B for a certain range of H_A values. Nevertheless T_1 has an end at $H_A = -H'_{C2}$ (cross in Fig. 1b) and a minimum appears in the FORC diagram as a consequence (Fig. 1c). We can assert that when a minimum appears just below a maximum value it likely signifies the end of the above transition. This result relates maxima and minima in the FORC density plot to transitions from a particular domain state, and whilst pairs of positive and negative points on the FORC diagram have been reported before [35,36], they are usually attributed to nucleation and annihilation processes in vortex and multidomain systems [37]. Indeed, the antiparallel configuration considered in this work is similar to a vortex state.

H_A values lower than $-H'_{C2}$ always exhibit a switching field for NS_1 at $H_B \geq H_{C1} - H_{int}$. Therefore, the FORC density plots a maximum corresponding to T_2, but no minimum will be seen below it, i.e., T_2 has no negative pair. Importantly, both T_1 and T_2 represent the minimum field required to switch the magnetization of NS_1 back to the initial (positive) state, but due to magnetostatic interactions, the switching field is different if going from the parallel to antiparallel configuration than in the opposite direction. We have shown, therefore, that FORC diagrams clearly allow us to distinguish both switching fields for the same nanostructure.

The distance between the T_1 minimum (cross) and the maximum T_2 (circle) is twice the mean interacting field, as shown in Fig. 2c with the double headed arrow. We suggest that this signal in the FORC diagram could be used to experimentally determine the mean interaction field between two NS, such as the experimental results presented by Groß et al. [31] to which the results in Fig. 2 show a remarkable similarity. Using this approach and the data shown in Fig. 2 of Groß et al. [31], we estimate the mean interacting field to be $H_{int} \sim 0.4$ Oe. The intrinsic coercive fields of the isolated NS can also be recovered from the FORC diagram of the two interacting NS. The intrinsic coercive field of the 30 μm strip in [31] can be calculated with this methodology as $H_C \sim 1.5$ Oe; the measured value is ~ 1.25 Oe (Fig. 1 of [31]).

The maximum T_3 represents the switching field of NS_2. This switching field is modified by the interaction field as $H'_{C2} = H_{C2} + H_{int}$. However, it is still possible to recover the intrinsic coercive field of NS_2, because the interacting field can be determined as described above. We estimate the intrinsic coercive field of the 10 μm stripe in [31] to be ~ 2.6 Oe, compared to the measured value of ~ 2.2 Oe (Fig. 1 in [31]). We have assumed the mean interaction field is acting equally on both NS, therefore, there is a small inherent inaccuracy in our estimation of the coercive fields of the 30 and 10 μm stripes in [31]; the interaction field of the wider NS is stronger than its corresponding counterpart. Assuming that interaction field produced by the 30 μm stripe is three times stronger than the one of the 10 μm stripe, the intrinsic coercive fields are $H_C \sim 1.3$ Oe and $H_C \sim 2.4$ Oe respectively, which is slightly closer to the measured value of ~ 2.2 Oe (Fig. 1 in [31]).

The strategy presented above can be applied to more complex systems such as the coreshell microwire presented in [33]. In this case the mean interacting field is $H_{int} \sim 1.5$ mT. However, the origin of this

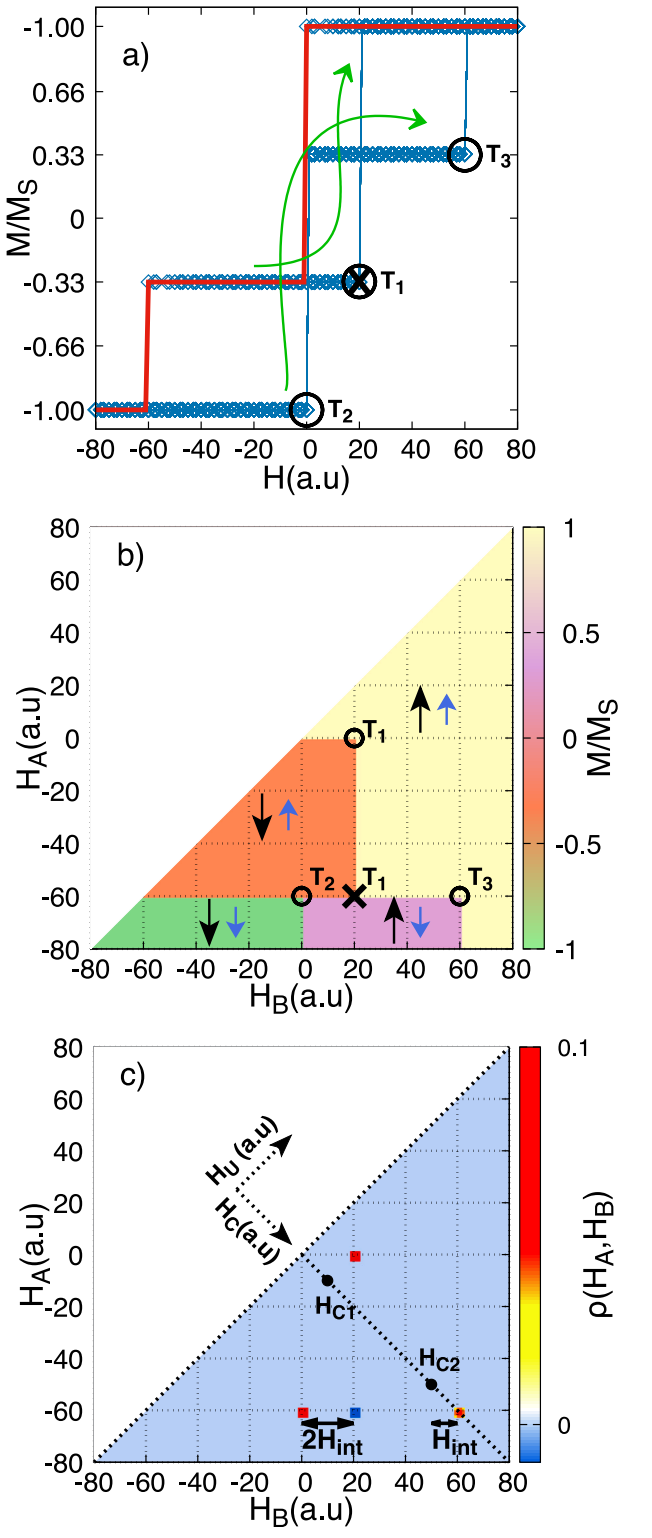

Fig. 2. Interacting case. (a) Magnetization versus field in a hysteresis loop like plot. The red line depicts the upper branch of the hysteresis loop, and the blue line and symbols the FORCs. (b) Magnetization colormap in terms of the applied field (H_A) and the FORC (H_B). The upper white triangle is outside measurement space. Arrow pairs indicates the magnetic state of the system in the corresponding color region. Black and blue arrow correspond to NS_1 and NS_2 respectively. Black circles highlight the starting H_A and H_B values required to produce a magnetic transition (T_1, T_2 or T_3). The black cross highlights the H_A and H_B fields at which T_1 ends. (c) FORC density plot; interaction H_U and coercive axes H_C are displayed for completeness. Double-headed arrows indicated the effect of the interaction. For comparison the non-interaction maxima (Fig. 1c) are plotted as black dots.

field is not necessary from the magnetostatic energy alone, but likely includes a weak negative exchange interaction between the inner wire and the shell.

In this work we do not observe any 'noisy tails' as are commonly seen experimentally [31]. This is because our model is an exact analytical model. In contrast, in FORC experiments, below a maximum there will almost always exists a repeatability error in the determination of H_B field at which the magnetic transition indicated by the maximum above occurs. This will give rise to a tail of random maxima and minima for a range of H_a values like if the transition is continuously ended and resumed. This is important because often such area of noise is filtered out, whereas in fact it constraints useful information for the existence of a domain transition. In experimental data we might expect to see such tails below each maxima, and its absence might then indicate a false maxima.

4. Conclusions

We have performed an analytic study of a very simple and well-defined magnetic system consisting of two elongated parallel magnetic nanostructures. We have calculated FORC diagrams for both non-interacting and interacting cases. In both cases maxima in the FORC density plots are due to the beginning of irreversible magnetic transitions (Figs. 1 & 2). For the interacting case, we have shown that a minimum that appears below a maximum (i.e., differing H_A fields and the same H_B field) likely identifies the end of the above transition. When a transition starts at a different H_B field value, but the same H_A, then an extra maximum appears in the FORC diagram. The distance of between the minimum and the new maximum represents approximately twice the mean interacting field. Using this interpretation the mean interaction field between two nanostructures can be determined.

There is the potential that this FORC diagram analysis could be extended to other slightly more complicated systems than the one considered here. In [33] the FORC diagram structure exhibited by a coreshell microwire is very similar to the one presented in this work, where NS_1 and NS_2 are replaced by the inner and outer shells. In that system, the dominant interaction field is most likely due to the exchange coupling. Nonetheless, the interaction strength can be measured within the procedure presented in this work.

CRediT authorship contribution statement

R. Moreno: Lead the work done in this paper, Reviewed the manuscript. **W. Williams:** Lead the work done in this paper, Reviewed the manuscript. **A.R. Muxworthy:** Lead the work done in this paper, Reviewed the manuscript. **G.A. Paterson:** Contributed the main ideas, Analyzed the results, Reviewed the manuscript. **D. Heslop:** Contributed the main ideas, Analyzed the results, Reviewed the manuscript.

Declaration of competing interest

The authors declare that they have no known competing financial interests or personal relationships that could have appeared to influence the work reported in this paper.

Data availability

Data will be made available on request.

Acknowledgments

This work was funded by Natural Environment Research Council Grants (NERC) NE/S011978/1 to W.W. and NE/S001018/1 to A.R.M. and W.W.. G.A.P. is supported by NERC Independent Research Fellowship NE/P017266/1 and D.H. is supported by Australian Research Council grant DP200100765.

References

[1] C.R. Pike, A.P. Roberts, K.L. Verosub, Characterizing interactions in fine magnetic particle systems using first order reversal curves, J. Appl. Phys. 85 (9) (1999) 6660–6667, http://dx.doi.org/10.1063/1.370176.

[2] A.P. Roberts, C.R. Pike, K.L. Verosub, First-order reversal curve diagrams: A new tool for characterizing the magnetic properties of natural samples, J. Geophys. Res. Solid Earth 105 (B12) (2000) 28461–28475, http://dx.doi.org/10.1029/2000JB900326, URL https://agupubs.onlinelibrary.wiley.com/doi/pdf/10.1029/2000JB900326, https://agupubs.onlinelibrary.wiley.com/doi/abs/10.1029/2000JB900326.

[3] M.I. Oliva, P.G. Bercoff, H.R. Bertorello, First order reversal curves analysis of the temperature effect on magnetic interactions in barium ferrite with La–Co addition, Physica B 404 (18) (2009) 2742–2745, http://dx.doi.org/10.1016/j.physb.2009.06.134, URL https://www.sciencedirect.com/science/article/pii/S0921452609004335.

[4] M. Pohlit, P. Eibisch, M. Akbari, F. Porrati, M. Huth, J. Müller, First order reversal curves (FORC) analysis of individual magnetic nanostructures using micro-hall magnetometry, Rev. Sci. Instrum. 87 (11) (2016) 113907, http://dx.doi.org/10.1063/1.4967940, URL https://aip.scitation.org/doi/pdf/10.1063/1.4967940, https://aip.scitation.org/doi/abs/10.1063/1.4967940.

[5] P. Tiberto, F. Celegato, G. Barrera, M. Coisson, F. Vinai, P. Rizzi, Magnetization reversal and microstructure in polycrystalline Fe50Pd50 dot arrays by self-assembling of polystyrene nanospheres, Sci. Technol. Adv. Mater. 17 (1) (2016) 462–472, http://dx.doi.org/10.1080/14686996.2016.1201414, pMID: 27877896.

[6] L.C.C. Arzuza, V. Vega, V.M. Prida, K.O. Moura, K.R. Pirota, F. Béron, Single diameter modulation effects on Ni nanowire array magnetization reversal, Nanomaterials 11 (12) (2021) http://dx.doi.org/10.3390/nano11123403, URL https://www.mdpi.com/2079-4991/11/12/3403.

[7] H. Mamiya, H. Fukumoto, J.L. Cuya Huaman, K. Suzuki, H. Miyamura, J. Balachandran, Estimation of magnetic anisotropy of individual magnetite nanoparticles for magnetic hyperthermia, ACS Nano 14 (7) (2020) 8421–8432, http://dx.doi.org/10.1021/acsnano.0c02521.

[8] M. Chiba, S. Kobayashi, T. Murakami, J. Manjanna, J. Szpunar, Temperature dependence of magnetic first-order-reversal-curves for hollow Fe3O4 submicron particles, AIP Adv. 9 (2019) 035235, http://dx.doi.org/10.1063/1.5080104.

[9] E.M. Palmero, M. Méndez, S. González, C. Bran, V. Vega, M. Vázquez, V.M. Prida, Stepwise magnetization reversal of geometrically tuned in diameter Ni and FeCo bi-segmented nanowire arrays, Nano Res. 12 (7) (2019) 1547–1553, http://dx.doi.org/10.1007/s12274-019-2385-9.

[10] R. Egli, Theoretical aspects of dipolar interactions and their appearance in first-order reversal curves of thermally activated single-domain particles, J. Geophys. Res. Solid Earth 111 (B12) (2006) http://dx.doi.org/10.1029/2006JB004567, URL https://agupubs.onlinelibrary.wiley.com/doi/pdf/10.1029/2006JB004567, https://agupubs.onlinelibrary.wiley.com/doi/abs/10.1029/2006JB004567.

[11] A.R. Muxworthy, A.P. Roberts, First-Order Reversal Curve (FORC) Diagrams, Springer, Netherlands, Dordrecht, 2007, pp. 266–272, http://dx.doi.org/10.1007/978-1-4020-4423-6_99.

[12] C.-I. Dobrotă, A. Stancu, What does a first-order reversal curve diagram really mean? A study case: Array of ferromagnetic nanowires, J. Appl. Phys. 113 (4) (2013) 043928, http://dx.doi.org/10.1063/1.4789613.

[13] S. Ruta, O. Hovorka, P.-W. Huang, K. Wang, G. Ju, R. Chantrell, First order reversal curves and intrinsic parameter determination for magnetic materials; limitations of hysteron-based approaches in correlated systems, Sci. Rep. 7 (2016) http://dx.doi.org/10.1038/srep45218.

[14] A. Stancu, P. Andrei, L. Stoleriu, Magnetic characterization of samples using first- and second-order reversal curve diagrams, J. Appl. Phys. 99 (2006) 08D702, http://dx.doi.org/10.1063/1.2172539.

[15] R. Harrison, X. Zhao, P. Hu, T. Sato, D. Heslop, A. Muxworthy, H. Oda, v.s.c. Kuppili, A. Roberts, Simulation of remanent, transient, and induced first-order reversal curve (FORC) diagrams for interacting particles with uniaxial, cubic, and hexagonal anisotropy, J. Geophys. Res. Solid Earth 124 (2019) http://dx.doi.org/10.1029/2019JB018050.

[16] A. Roberts, D. Heslop, X. Zhao, H. Oda, R. Egli, R. Harrison, P. Hu, A. Muxworthy, T. Sato, Unlocking information about fine magnetic particle assemblages from first-order reversal curve diagrams: Recent advances, Earth-Sci. Rev. (2022) 103950, http://dx.doi.org/10.1016/j.earscirev.2022.103950.

[17] X. Zhao, A.P. Roberts, D. Heslop, G.A. Paterson, Y. Li, J. Li, Magnetic domain state diagnosis using hysteresis reversal curves, J. Geophys. Res. Solid Earth 122 (7) (2017) 4767–4789, http://dx.doi.org/10.1002/2016JB013683, URL https://agupubs.onlinelibrary.wiley.com/doi/pdf/10.1002/2016JB013683, https://agupubs.onlinelibrary.wiley.com/doi/abs/10.1002/2016JB013683.

[18] R. Day, M. Fuller, V. Schmidt, Hysteresis properties of titanomagnetites: Grain-size and compositional dependence, Phys. Earth Planet. Inter. 13 (4) (1977) 260–267, http://dx.doi.org/10.1016/0031-9201(77)90108-X, URL https://www.sciencedirect.com/science/article/pii/003192017790108X.

[19] D.J. Dunlop, Theory and application of the day plot (Mrs/Ms versus Hcr/Hc) 1. Theoretical curves and tests using titanomagnetite data, J. Geophys. Res. Solid Earth 107 (B3) (2002) EPM 4–1–EPM 4–22, http://dx.doi.org/10.1029/2001JB000486, URL https://agupubs.onlinelibrary.wiley.com/doi/pdf/10.1029/2001JB000486, https://agupubs.onlinelibrary.wiley.com/doi/abs/10.1029/2001JB000486.

[20] E.M. Palmero, R. Salikhov, U. Wiedwald, C. Bran, M. Spasova, M. Vázquez, M. Farle, Enhanced magnetocrystalline anisotropy of $Fe_{30}Co_{70}$ nanowires by Cu additives and annealing, Nanotechnology 27 (36) (2016) 365704, http://dx.doi.org/10.1088/0957-4484/27/36/365704.

[21] X. Zhao, D. Heslop, A.P. Roberts, A protocol for variable-resolution first-order reversal curve measurements, Geochem. Geophys. Geosyst. 16 (5) (2015) 1364–1377, http://dx.doi.org/10.1002/2014GC005680, URL https://agupubs.onlinelibrary.wiley.com/doi/pdf/10.1002/2014GC005680, https://agupubs.onlinelibrary.wiley.com/doi/abs/10.1002/2014GC005680.

[22] K. Son, G. Schütz, E. Goering, Effect of the soft layer thickness on magnetization reversal process of exchange-spring nanomagnet patterns, Curr. Appl. Phys. 20 (4) (2020) 477–483, http://dx.doi.org/10.1016/j.cap.2020.01.014, URL https://www.sciencedirect.com/science/article/pii/S1567173920300146.

[23] A. Muxworthy, D. Heslop, W. Williams, Influence of magnetostatic interactions on first-order-reversal-curve (FORC) diagrams: A micromagnetic approach, Geophys. J. Int. 158 (3) (2004) 888–897, http://dx.doi.org/10.1111/j.1365-246X.2004.02358.x, URL https://academic.oup.com/gji/article-pdf/158/3/888/5987716/158-3-888.pdf.

[24] R. Egli, A.P. Chen, M. Winklhofer, K.P. Kodama, C.-S. Horng, Detection of noninteracting single domain particles using first-order reversal curve diagrams, Geochem. Geophys. Geosyst. 11 (1) (2010) http://dx.doi.org/10.1029/2009GC002916, URL https://agupubs.onlinelibrary.wiley.com/doi/pdf/10.1029/2009GC002916, https://agupubs.onlinelibrary.wiley.com/doi/abs/10.1029/2009GC002916.

[25] I. Lascu, J.F. Einsle, M.R. Ball, R.J. Harrison, The vortex state in geologic materials: A micromagnetic perspective, J. Geophys. Res. Solid Earth 123 (9) (2018) 7285–7304, http://dx.doi.org/10.1029/2018JB015909, URL https://agupubs.onlinelibrary.wiley.com/doi/pdf/10.1029/2018JB015909, https://agupubs.onlinelibrary.wiley.com/doi/abs/10.1029/2018JB015909.

[26] C. Carvallo, A.P. Roberts, R. Leonhardt, C. Laj, C. Kissel, M. Perrin, P. Camps, Increasing the efficiency of paleointensity analyses by selection of samples using first-order reversal curve diagrams, J. Geophys. Res. Solid Earth 111 (B12) (2006) B12103, http://dx.doi.org/10.1029/2005JB004126.

[27] L. Nagy, W. Williams, A.R. Muxworthy, K. Fabian, T.P. Almeida, P.O. Conbhuí, V.P. Shcherbakov, Proc. Natl. Acad. Sci. 114 (39) (2017) 10356–10360, http://dx.doi.org/10.1073/pnas.1708344114, URL https://www.pnas.org/content/114/39/10356.full.pdf, https://www.pnas.org/content/114/39/10356.

[28] L. Néel, Remarques sur la théorie des propriétés magnétiques des substances dures, Appl. Sci. Res. B 4 (1955) 13–24.

[29] A. Muxworthy, W. Williams, Magnetostatic interaction fields in first-order-reversal-curve diagrams, J. Appl. Phys. 97 (6) (2005) http://dx.doi.org/10.1063/1.1861518.

[30] A.R. Muxworthy, J.G. King, D. Heslop, Assessing the ability of first-order reversal curve (FROC) diagrams to unravel complex magnetic signals, J. Geophys. Res. Solid Earth 110 (B1) (2005) http://dx.doi.org/10.1029/2004JB003195, URL https://agupubs.onlinelibrary.wiley.com/doi/pdf/10.1029/2004JB003195, https://agupubs.onlinelibrary.wiley.com/doi/abs/10.1029/2004JB003195.

[31] F. Groß, S.E. Ilse, G. Schütz, J. Gräfe, E. Goering, Interpreting first-order reversal curves beyond the Preisach model: An experimental permalloy microarray investigation, Phys. Rev. B 99 (2019) 064401, http://dx.doi.org/10.1103/PhysRevB.99.064401, URL https://link.aps.org/doi/10.1103/PhysRevB.99.064401.

[32] V. Kolesnikova, J. Martínez-García, V. Rodionova, M. Rivas, Study of bistable behaviour in interacting Fe-based microwires by first order reversal curves, J. Magn. Magn. Mater. 508 (2020) 166857, http://dx.doi.org/10.1016/j.jmmm.2020.166857, URL https://www.sciencedirect.com/science/article/pii/S0304885319337941.

[33] C. Yang, Y. Kita, Z. Song, Y. Takemura, Magnetic reversal in Wiegand wires evaluated by first-order reversal curves, Materials 14 (14) (2021) 3868, http://dx.doi.org/10.3390/ma14143868, pMID: 34300787, URL https://pubmed.ncbi.nlm.nih.gov/34300787.

[34] D. Heslop, A. Muxworthy, Aspects of calculating first-order reversal curve distributions, J. Magn. Magn. Mater. 288 (2005) 155–167, http://dx.doi.org/10.1016/j.jmmm.2004.09.002.

[35] C. Pike, A. Fernandez, An investigation of magnetic reversal in submicron-scale Co dots using first order reversal curve diagrams, J. Appl. Phys. 85 (9) (1999) 6668–6676.

[36] R.K. Dumas, C.-P. Li, I.V. Roshchin, I.K. Schuller, K. Liu, Magnetic fingerprints of sub-100 nm Fe dots, Phys. Rev. B 75 (13) (2007) 134405.

[37] A.P. Roberts, D. Heslop, X. Zhao, C.R. Pike, Understanding fine magnetic particle systems through use of first-order reversal curve diagrams, Rev. Geophys. 52 (4) (2014) 557–602, http://dx.doi.org/10.1002/2014rg000462.